

Vibrational Spectroscopic and Molecular Docking Studies of Amrinone, a Cardiotonic Inotropic Drug

© Sefa Celik¹, Sevim Akyuz², Aysen E. Ozel¹, and Elif Akalin¹

¹ Physics Department, Science Faculty, Istanbul University, Vezneciler, 34134, Istanbul, Turkey

² Physics Department, Science and Letters Faculty, Istanbul Kultur University, Atakoy Campus, Bakirkoy 34156, Istanbul, Turkey

e-mail: scelik@istanbul.edu.tr

Received April 29, 2021

Revised April 29, 2021

Accepted September 30, 2021

Amrinone is a class I cardiotonic inotropic agent, which is known to increase the cyclic adenosine monophosphate (cAMP) level by inhibiting the phosphodiesterase 3 (PDE3) enzyme. In this study the theoretically possible stable conformations of the amrinone, was examined first by conformational analysis method and then the obtained most stable conformation was optimized by DFT/wb97xd/6-311++G(d,p) level of theory using Gaussian 03 program. The credibility of the theoretical model was confirmed by comparison of experimental and theoretical vibrational spectra of the title molecule. The fundamental vibrational wavenumbers, IR and Raman intensities of the optimized structure of amrinone were determined using DFT/wb97xd/6-311++G(d,p) level of theory and compared with the experimental vibrational spectra. To investigate the influence of amrinone on cAMP enhancement, the docking simulations towards PDE3B were carried out and the main binding interactions of amrinone with PDE3 were elucidated. Cytochrome P450s (CYPs) are very important phase I metabolizing enzymes. The interaction between amrinone and CYPs (CYP1A2, CYP2C9 and CYP2C19) was investigated by docking simulations. Moreover, molecular docking of the title molecule with different proteins and receptors were studied to reveal potential mechanisms for therapeutic applications. Molecular docking simulations revealed that amrinone showed strong binding affinity to integrins $\alpha_5\beta_1$ ($\Delta G = -6.6$ kcal/mol) and $\alpha_{IIb}\beta_3$ (-6.6 kcal/mol), and DNA (-6.5 kcal/mol). The results correlated with its anticancer activity. The drug likeness and ADMET properties of amrinone were analyzed for the prediction of pharmacokinetic profiles.

Key words: amrinone, DFT calculations, FTIR, molecular docking, ADMET.

Introduction

Amrinone (5-amino-[3,4'-bipyridinyl-6(1H)-one; C₁₀H₉N₃O) is used as a cardiotonic drug and is a class I cardiotonic inotropic agent that increases the cellular levels of cyclic adenosine monophosphate [1]. Cardiovascular disorders are among the most common diseases today. Amrinone has been shown to have important biological activity in cardiovascular disorders by acting as an inhibitor of phosphodiesterase 3 (PDE3) enzyme [1,2]. It is a positive inotropic agent with vasodilatory activity. Amrinone increases muscle contractility by reducing the degradation of cyclic adenosine monophosphate (cAMP). Its vasodilatory effect is the result of its direct relaxing effect on vascular smooth muscle [1–3].

The three-dimensional structure of amrinone was investigated by Robertson et al. using X-Ray crystallographic and NMR (1H and 13C-NMR) studies [4]. The amrinone molecule was found to be almost planar in the crystalline state with the 1.3° torsion angle between the rings [4]. However, in this work, significant structural differences have also been suggested for the solution state compared to the crystalline phase, and authors proposed a twisted structure for amrinone in solution depending on 1H and 13C-NMR studies [4]. Following the study, Hofmann and Cimraglia (1987), carried out the conformational analysis of amrinone using STO-3G method, and found the torsion angle between

the two rings of amrinone as 37.13° [5]. In the same year XRD analysis of amrinone was performed by Cody (1987), and the presence of conformational flexibility in the amrinone structure in the crystal phase was reported [6]. In the crystal structure, four independent amrinone molecules having four different torsion angles between the rings were revealed and the torsion angles were found to be $-13.4(9)^\circ$, $-11.8(10)^\circ$, $-8.7(10)^\circ$ and $-21.7(10)^\circ$ [6].

Amrinone belongs to the bipyridine class of organic compounds. It is 3,4'-bipyridine substituted by an amino and carbonyl group at 5 and 6 positions, respectively. Recently IR, Raman spectroscopic study on milrinone, which is another bipyridine class of molecule, also a phosphodiesterase-3 inhibitor, was reported [7].

The principle aim of this study is to elucidate the binding affinity and the main binding interactions of amrinone with PDE3. Since function-conformation relation is important for bioactive molecules, a combined experimental and theoretical study on molecular structure and vibrational spectra of amrinone was also carried out to confirm the credibility of the theoretical model molecular structure. Early studies in patients with heart failure showed that amrinone produced short-term hemodynamic improvement but had limited long-term clinical benefit [1]. Drug metabolism primarily mediated by P450-family cytochromes (CYP). For this reason, the interaction of amrinone with CYP1A2, CYP2C9 and CYP2C19 was investigated by docking simulations. It

is important to shed light on the potential mechanisms of amrinone for therapeutic applications since it has good absorption from the gastrointestinal tract and less toxicity. Therefore, the interaction of the molecule with integrins and DNA, to reveal its anticancer potential, has been studied.

1. Experimental and computational procedures

1.1. Experimental

Amrinone in the solid form was purchased from the Sigma-Aldrich Chemical Company (CAS Number 60719-84-8) with reagent grade and was used as received. The IR spectrum of the KBr disc of amrinone was recorded on a Bruker Tensor 27 FT-IR spectrometer with 1 cm^{-1} resolution in the region 400 and 4000 cm^{-1} . The Raman spectrum of the sample was recorded with a Jasco NRS 3100 micro-Raman spectrometer having a 532-nm diode laser and a diffraction grating of 1200 lines/mm in the $1950\text{--}50\text{ cm}^{-1}$ region. The spectrometer was calibrated with silicon phonon mode at 520 cm^{-1} .

1.2. Computational details

The theoretically possible stable conformations of the amrinone, was examined first by conformational analysis method using SPARTAN program [8] using DFT/B3LYP-6-31G(d,p) level of theory and then the most stable conformation obtained was optimized by DFT/wb97xd/6-311++G(d,p) level of theory using Gaussian 03 program [9,10].

The vibrational wavenumbers of the lowest energy conformation obtained was calculated at the DFT/wb97xd/6-311++G(d,p) level of theory. The harmonic force field of the most stable conformation of amrinone molecule was evaluated by scaled quantum mechanical force field method [11] using the MOLVIB program, and the IR density, Raman activity, and the potential energy distributions of the vibrational modes (PED) were determined by converting the Cartesian coordinate force fields to natural internal coordinates [12,13]. The Raman activities have been converted to Raman intensities with the help of Simirra program [14]. The calculated IR and Raman spectra were simulated using Lorentzian band shapes with a bandwidth (FWHM) of 10 cm^{-1} .

The scale factors used for the wavenumbers computed by DFT/wb97xd/6-311++G(d,p) level of theory in order to give the best fit to the experimental data, are as follows:

- N–H stretch 0.89,
- C=O stretch 0.88,
- C–H stretch 0.91,
- N–H and C–H deformation 0.90,
- all others 0.98.

For docking studies the crystal structure of human phosphodiesterase 3 (PDE3), DNA, $\alpha_5\beta_1$ and $\alpha_{11b}\beta_3$ integrins, CYP1A2, CYP2C9 and CYP2C19 human cytochromes

P450 were obtained from the protein data bank (PDB IDs: 1SO2, 1BNA, 4WK0, 3ZDX, 2HI4, 1R9O, 4GQS, respectively) [15–21]. Molecular docking simulations were performed by the Autodock Vina program [22] and binding affinities were calculated. The active sites of receptors were screened by using the CAVER program [23]. The partial charges of amrinone molecule were calculated using the Geistenger method. Target molecules were adapted for docking by removing the water molecule from the receptors and adding polar hydrogens. The active sites of the target proteins and DNA were defined in the grid size of $40\text{ \AA} \times 40\text{ \AA} \times 40\text{ \AA}$.

The toxicological risk and physicochemical properties of the amrinone were obtained using the OSIRIS property explorer [24]. The ADMET (absorption, distribution, metabolism, excretion and toxicity) properties of the title molecule, from its optimized structure, were predicted using ADMET SAR [25].

2. Results and discussion

2.1. Molecular geometric structure

The initial geometry parameters of amrinone were taken from the crystal structure [6]. The conformational analysis of the molecule was performed first and the lowest energy among the molecular structures obtained was optimized. As a result of the optimization of the lowest energy conformers of amrinone obtained by conformation analysis at DFT/wb97xd/6-311++G(d,p) theory level. The minimum energy conformer of amrinone was found to have $-392775.58\text{ kcal/mol}$ of energy. The optimization of the most stable conformer was then repeated by rotating the NH_2 group, however, in this case the $-392775.53\text{ kcal/mol}$ energy was obtained (there is a 0.05 kcal/mol increase in energy), so no more decrease in energy was observed. The obtained molecular structure of these two low energy conformers of amrinone is presented in Fig. 1. For the further calculations the geometry parameters of amrinone shown in Fig. 1, *a* were used.

The geometric parameters of the most stable conformer of amrinone having $-392775.58\text{ kcal/mol}$ energy is given in Table 1. The dihedral angle between the pyridine rings D(5,4,14,19) is found to be -39.6° . In the crystallographic study on amrinone, for four independent amrinone molecules, the orientation of the two pyridine rings were reported as $-13.4(9)^\circ$, $-11.8(10)^\circ$, $-8.7(10)^\circ$ and $-21.7(10)^\circ$. Hofmann and Cimraglia (1987) found the twist angle 37.1° as a result of their conformational analysis on amrinone with the *ab initio* STO-3G method [5]. On the other hand, Bhattacharjee (1990) had estimated this angle as 37° by performing conformational analysis using the *ab initio* molecular orbital theory at STO-3G and 3-21G levels [26]. Thus, our result is consistent with the previous findings.

As seen in Table 1, the calculated bond length of the C–C bonds of the optimized amrinone molecule varies

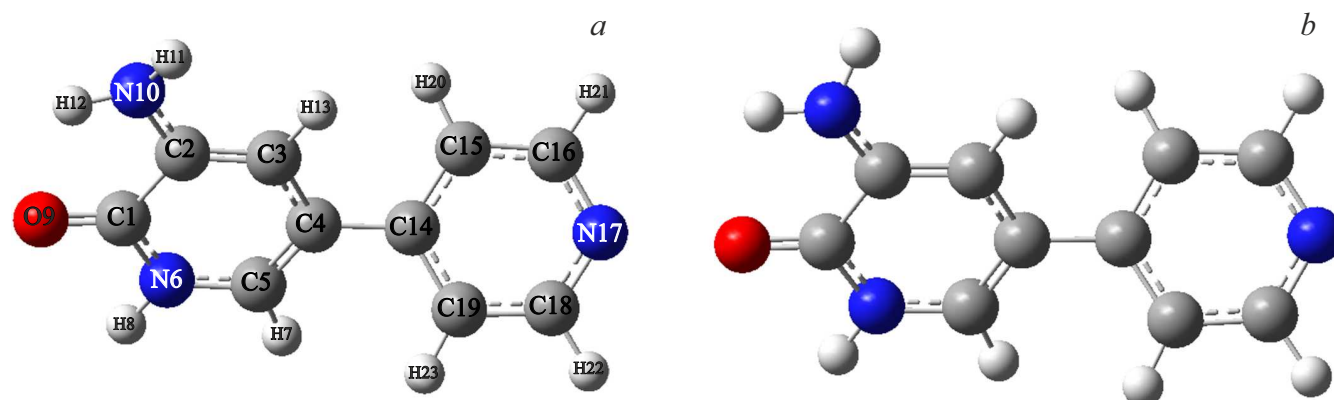


Figure 1. The optimized molecular structure of amrinone with atomic numbering scheme obtained using DFT/wb97xd/6-311++G(d,p) level of theory, $E = -392775.58$ kcal/mol (a), the second low energy conformer, obtained by rotation of NH_2 group, $E = -392775.53$ kcal/mol (b).

Table 1. Geometric parameters (bond length (Å)/bond angle ($^\circ$)) for amrinone

Atoms		Atoms		Atoms		Atoms	
R(1,2)	1.467	R(15,20)	1.084	A(3,4,14)	120.9	A(15,16,17)	124.0
R(1,6)	1.376	R(16,17)	1.332	A(5,4,14)	120.8	A(15,16,21)	120.0
R(1,9)	1.224	R(16,21)	1.086	A(4,5,6)	120.0	A(17,16,21)	116.1
R(2,3)	1.363	R(17,18)	1.332	A(4,5,7)	123.8	A(16,17,18)	116.6
R(2,10)	1.371	R(18,19)	1.388	A(6,5,7)	116.2	A(17,18,19)	123.9
R(3,4)	1.432	R(18,22)	1.087	A(1,6,5)	125.6	A(17,18,22)	116.0
R(3,13)	1.085	R(19,23)	1.084	A(1,6,8)	114.5	A(19,18,22)	120.0
R(4,5)	1.357	A(2,1,6)	114.4	A(5,6,8)	119.8	A(14,19,18)	119.3
R(4,14)	1.478	A(2,1,9)	123.5	A(2,10,11)	118.5	A(14,19,23)	120.8
R(5,6)	1.371	A(6,1,9)	122.1	A(2,10,12)	114.5	A(18,19,23)	119.9
R(5,7)	1.081	A(1,2,3)	120.2	A(11,10,12)	116.4	D(3,4,14,15)	-38.4
R(6,8)	1.010	A(1,2,10)	113.9	A(4,14,15)	121.3	D(3,4,14,19)	141.8
R(10,11)	1.005	A(3,2,10)	125.9	A(4,14,19)	121.9	D(5,4,14,15)	140.2
R(10,12)	1.010	A(2,3,4)	121.6	A(15,14,19)	116.8	D(5,4,14,19)	-39.60
R(14,15)	1.395	A(2,3,13)	119.5	A(14,15,16)	119.3		
R(14,19)	1.396	A(4,3,13)	118.9	A(14,15,20)	120.9		
R(15,16)	1.388	A(3,4,5)	118.2	A(16,15,20)	119.8		

between 1.467–1.357 Å. The average C–C bond lengths of the pyridinone rings of four amrinone molecules in the amrinone crystal were found between 1.425 (8)–1.358 (8) Å in the experimental XRD study [6]. The central bond length of amrinone (distance between the rings) was calculated as 1.506 Å by Hofmann and Cimiraaglia (1987) [5], whereas, it was found to be 1.477 Å [6,7] experimentally. In our study the bond length between the rings of amrinone $\{R(4, 14)\}$ was calculated to be 1.478 Å, and its experimental value is 1.477 Å [6,7]. The C=O bond length $\{R(1, 9)\}$ is calculated to be 1.224 Å, which is consistent with the experimental C=O bond length of 2-pyridinone (1.2531 Å) [27].

In the optimized structure of amrinone, the calculated value of the angle between atoms numbered 4,5 and 7 $\{A(4, 5, 7)\}$ is 123.8° (Table 1). This was referred to as α by Hofmann and Cimiraaglia (1987) and calculated to be 124.48° [5].

The angles between atoms numbered 4,3,13 $\{A(4, 3, 13)\}$, atoms numbered 14,15,20 $\{A(14, 15, 20)\}$ and atoms numbered 14,19,23 $\{A(14, 19, 23)\}$ are predicted as 118.9°, 120.9° and 120.8°, respectively (Table 1). These angles were referred to as β , γ , and δ , respectively, by Hofmann and Cimiraaglia (1987) and calculated to be 117.9°, 121.23° and 121.15°, respectively [5]. Our results are consistent with previous findings.

2.2. Vibrational spectra

Amrinone has 23 atoms, therefore has 63 normal vibrations. The molecule has C_1 symmetry, so all the modes are IR and Raman active.

In this study the vibrational wavenumbers of the most stable conformer of amrinone molecule were calculated at the DFT/wb97xd/6-311++G(d,p) level of theory and compared with experimental values. The calculated and

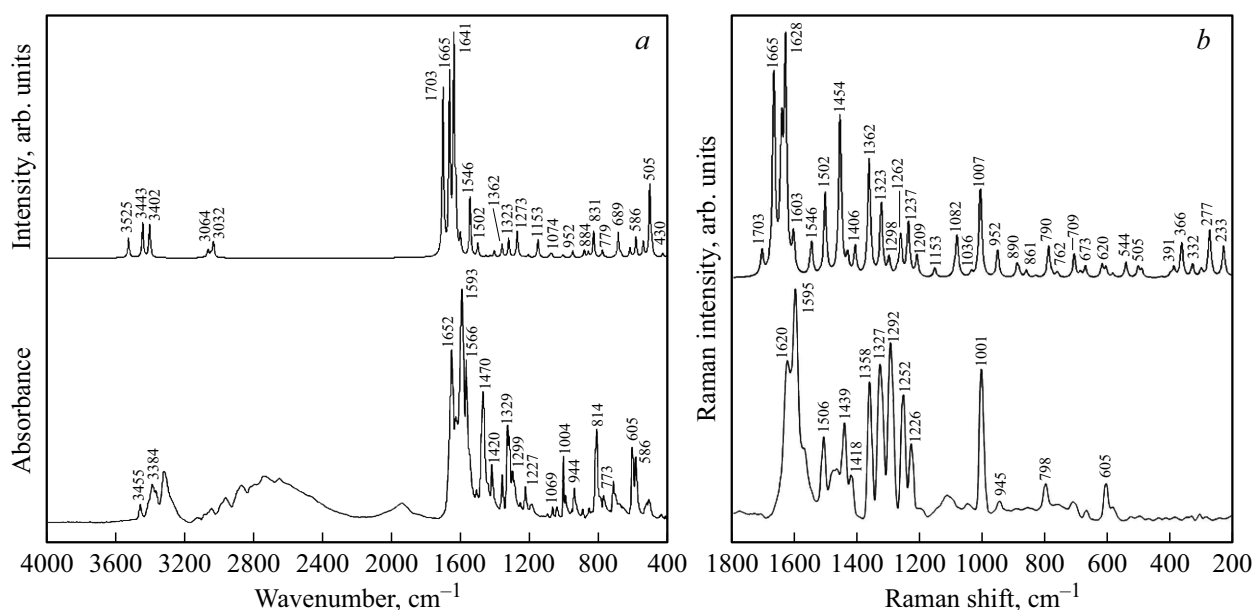


Figure 2. The experimental (bottom) and simulated (top) IR (a) and Raman (b) spectra of amrinone.

scaled wavenumbers of amrinone molecule in the gas phase together with the potential energy distribution of the vibrational modes (PED) are given in comparison with the experimental wavenumbers of solid amrinone in Table 2. The comparison of experimental and theoretical vibration spectra can be used to prove the accuracy of the calculated molecular structure. No imaginary wavenumber was obtained. Besides, the calculated wavenumbers were found to be in good agreement with the experimental values. The experimental FTIR and Raman spectra of amrinone are given in Fig. 2, a and 2, b, respectively, in comparison with their simulated spectra.

The NH stretching wavenumbers are expected to be in the $3500\text{--}3200\text{ cm}^{-1}$ range. The amrinone molecule has an amino group and an N–H bond belonging to the 2-pyridone ring. The NH stretching band was not observed in solid phase of 2-pyridone but observed at 3396 cm^{-1} as a weak band in its chloroform solution [28]. The band at 3409 cm^{-1} , which is observed as a shoulder in the solid phase IR spectrum of amrinone but clearly detected in the second derivative profile of the absorption spectrum, is assigned to N–H (N6–H8) stretching vibration of 2-pyridone ring. This assignment is in accordance with the computed wavenumber at 3443 cm^{-1} with 100% PED contribution (Table 2). The N–H stretching wavenumber of the 2-pyridone ring of milrinone was observed at 3451 cm^{-1} in the FTIR spectrum [7].

The asymmetric and symmetric NH₂ stretching wavenumbers of aniline were observed at 3508 and 3422 cm^{-1} in the argon matrix [29], and at 3440 and 3360 cm^{-1} in liquid aniline [30], respectively. In our study the medium intense bands observed at 3455 and 3384 cm^{-1} were assigned to the asymmetric and symmetric NH₂ stretching wavenumbers of amrinone. These modes were computed to be 3525 and 3402 cm^{-1} , respectively,

by using the DFT/wb97xd/6-311++G(d,p) level of theory. It must be noted that calculation was performed for the free molecule in the gas phase and the IR spectrum was recorded for solid amrinone. It is known that NH bonds in solid phase are involved in H-bond interaction [6].

The C=O stretching vibration of 2-pyridone was observed at 1652 cm^{-1} as a very strong band and at 1648 cm^{-1} as a weak band in the IR and Raman spectra of the solid 2-pyridone, respectively, and observed at 1674 cm^{-1} in the IR spectrum of the 2-pyridone chloroform solution [28]. The very strong band at 1652 cm^{-1} observed in the IR spectrum of amrinone in this study is attributed to C=O stretching mode of 2-pyridone ring.

According to PED analysis, the NH₂ bending vibration of the amrinone molecule was a mixed-mode with ring NH bending and ring stretching vibrations at 1546 cm^{-1} . The strong band observed at 1566 cm^{-1} in the IR and the medium intense band observed at 1566 cm^{-1} in Raman spectra are attributable to this mode. The other amino group vibrations (such as NH₂ wagging and NH₂ rocking vibrations) were assigned according to computed PED values of amrinone and by taking the experimental aniline wavenumbers into account [31].

The ring vibrations of amrinone were assigned according to the computed wavenumbers and also to the experimental vibrational spectra of 2-pyridone [28] and pyridine [32].

A good correlation between experimental IR, Raman spectra, and the band positions of the computed spectra were obtained. The small differences between the observed and calculated wavenumbers may in a great part be due to the fact that the IR and Raman spectra of the compound have been measured in the solid phase and the calculations were performed on the isolated molecule in the gas phase. The mean absolute deviation, standard deviation, root mean square, and correlation coefficient (r) between

Table 2. The calculated (wb97xd/6-311++G(d,p)) and experimental wavenumbers (cm^{-1}) of amrinone and the PED distributions of the vibration modes

Assignment	Experimental		Calculated			PED%
	IR	Ra	wb97xd/6-311++G(d,p)			
			ν^s	I(IR)	I(Ra)	
$\nu_{a\text{NH}_2}$	3455m		3525	42	5	$\nu_{\text{NH}}(100)$
ν_{NH}	3409sh		3443	73	14	$\nu_{\text{NH}}(100)$
$\nu_{s\text{NH}_2}$	3384m		3402	71	22	$\nu_{\text{NH}}(100)$
ν_{CH}	3082w		3090	1	9	$\nu_{\text{CH}}(99)$
ν_{CH}	3065w		3067	3	28	$\nu_{\text{CH}}(96)$
ν_{CH}	3060w		3064	15	24	$\nu_{\text{CH}}(99)$
ν_{CH}			3049	8	12	$\nu_{\text{CH}}(98)$
ν_{CH}	3044w		3036	17	29	$\nu_{\text{CH}}(93)$
ν_{CH}	3029w		3032	23	29	$\nu_{\text{CH}}(100)$
$\nu_{\text{CC}} + \nu_{\text{C=O}}$	1669sh	1664sh	1703	349	12	$\nu_{\text{CO}}(26) + \nu_{\text{CC}}(37) + \nu_{\text{CN}}(6)$
$\nu_{\text{C=O}}$	1652vs		1665	370	85	$\nu_{\text{CO}}(41) + \nu_{\text{CC}}(24) + \nu_{\text{CN}}(6)$
ν_{CC}	1636sh		1641	443	69	$\nu_{\text{CO}}(7) + \nu_{\text{CC}}(48) + \nu_{\text{CN}}(5)$
ν_{CC}	1627s	1620vs	1628	111	100	$\nu_{\text{CN}}(19) + \nu_{\text{CC}}(44)$
ν_{CC}	1593vs	1595vs	1603	40	20	$\nu_{\text{CC}}(37) + \nu_{\text{CN}}(29)$
δ_{NH}	1566s	1566m	1546	126	15	$\delta_{\text{HNH}}(41) + \delta_{\text{CNH}}(28) + \nu_{\text{CC}}(13)$
ν_{CC}	1506w	1506s	1502	29	35	$\nu_{\text{CC}}(21) + \nu_{\text{CN}}(17) + \delta_{\text{CCH}}(7) + \delta_{\text{NCH}}(6)$
$\nu_{\text{CN}}(\text{ring})$	1470s	1460m	1454	3	67	$\nu_{\text{CN}}(21) + \delta_{\text{CNH}}(15) + \nu_{\text{CC}}(8) + \nu_{\text{CO}}(7)$
$\nu_{\text{CO}} + \nu_{\text{CC}} + \delta_{\text{NH}}$	1443s	1439s	1430	4	12	$\nu_{\text{CO}}(16) + \nu_{\text{CC}}(12) + \delta_{\text{CCH}}(9) + \delta_{\text{CNH}}(21)$
ν_{CC}	1420m	1418m	1406	14	14	$\nu_{\text{CC}}(32) + \delta_{\text{NCH}}(20) + \delta_{\text{CCH}}(6)$
ν_{CC}	1360m	1358vs	1362	27	49	$\nu_{\text{CC}}(37) + \nu_{\text{CN}}(22)$
ν_{CC}	1329s	1327vs	1323	40	31	$\nu_{\text{CC}}(19) + \delta_{\text{NCH}}(15) + \nu_{\text{CN}}(19) + \delta_{\text{CCH}}(10)$
δ_{CH}	1317s		1298	1	10	$\delta_{\text{CCH}}(42) + \delta_{\text{NCH}}(16)$
$\nu_{\text{CN}}(\text{ring}) + \nu_{\text{C-NH}_2}$	1299m	1292vs	1273	55	6	$\nu_{\text{CN}}(45) + \delta_{\text{CNH}}(23) + \nu_{\text{CC}}(6)$
$\nu_{\text{CN}}(\text{ring})$	1255w	1252s	1262	3	18	$\nu_{\text{CN}}(33) + \nu_{\text{CC}}(39)$
δ_{CH}	1227m	1226s	1237	3	24	$\delta_{\text{CCH}}(35) + \nu_{\text{CC}}(15) + \nu_{\text{CN}}(7)$
δ_{CH}	1193w	1191vw	1209	6	10	$\delta_{\text{NCH}}(32) + \delta_{\text{CCH}}(29) + \nu_{\text{CN}}(9)$
δ_{CH}		1144vw	1153	39	4	$\delta_{\text{NCH}}(19) + \delta_{\text{CCH}}(16) + \nu_{\text{CN}}(19) + \delta_{\text{CNH}}(10)$
δ_{CH}	1097vw	1097w	1090	1	8	$\delta_{\text{CCH}}(39) + \nu_{\text{CC}}(24)$
NH_2 rocking			1082	6	18	$\delta_{\text{CNH}}(27) + \delta_{\text{CCH}}(19) + \nu_{\text{CC}}(14)$
δ_{CH}	1069w	1073w	1074	8	6	$\delta_{\text{CCH}}(48) + \nu_{\text{CN}}(23)$
ν_{CC}	1042w	1045vw	1036	1	3	$\nu_{\text{CC}}(34) + \delta_{\text{CNH}}(28)$
γ_{CH}			1013	1	17	$\Gamma_{\text{HCCH}}(46) + \Gamma_{\text{CNCH}}(18) + \Gamma_{\text{CCCH}}(13)$
δ_{ring}	1004m	1001vs	1007	6	36	$\delta_{\text{CNC}}(11) + \nu_{\text{CN}}(16) + \delta_{\text{CCN}}(14) + \delta_{\text{CCC}}(7)$
γ_{CH}	959vw		989	0	3	$\Gamma_{\text{HCCH}}(54)$
δ_{ring}	944m	945w	952	15	12	$\delta_{\text{CCN}}(15) + \delta_{\text{CCC}}(18) + \nu_{\text{CN}}(10) + \delta_{\text{CNC}}(5)$
γ_{CH}	893vw		890	1	6	$\Gamma_{\text{NCC}}(24) + \Gamma_{\text{CCCH}}(42)$
γ_{CH}	871vw		884	16	5	$\Gamma_{\text{NCC}}(29) + \Gamma_{\text{CCCH}}(46)$
γ_{CH}	860vw		861	12	4	$\Gamma_{\text{CCCH}}(42) + \Gamma_{\text{HCNH}}(9) + \Gamma_{\text{HCNC}}(6)$
	856vw					
γ_{CH}	840vw		831	55	1	$\Gamma_{\text{CCCH}}(39) + \Gamma_{\text{HCNH}}(10) + \Gamma_{\text{CNCH}}(7)$
ν_{CC}	814s	798m	790	3	13	$\nu_{\text{CC}}(37) + \nu_{\text{CN}}(12) + \nu_{\text{CO}}(5)$
τ_{ring}	789vw		779	16	3	$\Gamma_{\text{OCNH}}(21) + \Gamma_{\text{OCCN}}(21) + \Gamma_{\text{CCCN}}(10) + \Gamma_{\text{CNCC}}(8) + \Gamma_{\text{CCCC}}(6)$
τ_{ring}	773w		762	1	3	$\Gamma_{\text{CCCN}}(20) + \Gamma_{\text{CCNC}}(20) + \Gamma_{\text{NCC}}(16)$
$\nu_{\text{CC}} + \delta_{\text{ring}}$	709w	707w	709	1	10	$\delta_{\text{CNC}}(24) + \nu_{\text{CC}}(24)$
γ_{NH}			689	53	3	$\Gamma_{\text{OCNH}}(28) + \Gamma_{\text{CCNH}}(36) + \Gamma_{\text{HCNH}}(15)$
δ_{ring}		667w	673	8	5	$\delta_{\text{CCN}}(34) + \delta_{\text{CCC}}(29)$
τ_{ring}	617sh		620	20	6	$\Gamma_{\text{CCCH}}(9) + \Gamma_{\text{OCNH}}(8) + \Gamma_{\text{CCCN}}(7) + \Gamma_{\text{CCNH}}(6) + \delta_{\text{CCC}}(10)$
δ_{CO}	605s	605m	607	2	5	$\delta_{\text{NCO}}(14) + \delta_{\text{CCO}}(10) + \nu_{\text{CN}}(10) + \delta_{\text{CCC}}(15) + \delta_{\text{CCN}}(7)$
δ_{ring}	586s	581w	586	43	2	$\delta_{\text{CNC}}(20) + \delta_{\text{CCO}}(9) + \delta_{\text{CCC}}(13) + \delta_{\text{CCN}}(7)$
δ_{ring}			544	32	7	$\delta_{\text{CCC}}(15) + \delta_{\text{CCN}}(6)$
NH_2 wagging	523w	523vw	505	152	5	$\Gamma_{\text{CCNH}}(43) + \delta_{\text{CNH}}(27) + \nu_{\text{CN}}(10) + \delta_{\text{HNH}}(10)$
δ_{ring}	509w		494	22	4	$\delta_{\text{NCO}}(14) + \delta_{\text{CCC}}(14) + \delta_{\text{CCN}}(18)$
τ_{ring}	440vw		430	8	1	$\Gamma_{\text{CCNH}}(31) + \Gamma_{\text{CCCO}}(7) + \Gamma_{\text{CCCH}}(12) + \Gamma_{\text{NCCN}}(5)$

Table 2. Continued.

Assignment	Experimental		Calculated			PED%
	IR	Raman	wb97xd/6-311++G(d,p)			
			ν^S	I(IR)	I(Raman)	
δ_{ring}			401	3	3	$\delta_{\text{CCC}}(24) + \Gamma_{\text{CNCO}}(6)$
τ_{ring}			391	0	5	$\Gamma_{\text{CCCN}}(34) + \Gamma_{\text{CCCH}}(22) + \Gamma_{\text{NCCH}}(12)$
τ_{ring}			366	116	15	$\Gamma_{\text{CCNH}}(48) + \delta_{\text{CNH}}(24) + \delta_{\text{HNH}}(9) + \nu_{\text{CN}}(7)$
δ_{ring}			332	23	6	$\delta_{\text{CCN}}(31) + \delta_{\text{CCO}}(10) + \delta_{\text{CNH}}(10) + \nu_{\text{CN}}(7) + \delta_{\text{HNH}}(6)$
δ_{ring}		305vw	304	7	4	$\delta_{\text{CCC}}(17) + \delta_{\text{CCN}}(13)$
$\nu_{\text{CC}} + \delta_{\text{ring}}$		270vw	277	1	20	$\nu_{\text{CC}}(32) + \delta_{\text{CCC}}(22)$
τ_{ring}		239vw	233	9	13	$\Gamma_{\text{CCCN}}(11)$
τ_{ring}			159	5	18	$\Gamma_{\text{NCCO}}(12) + \Gamma_{\text{CCCO}}(12) + \Gamma_{\text{NCCC}}(9) + \Gamma_{\text{OCNC}}(9) + \Gamma_{\text{NCCN}}(8) + \Gamma_{\text{CCNC}}(6)$
δ_{ring}			103	2	49	$\delta_{\text{CCC}}(62)$
τ_{ring}			69	3	118	$\Gamma_{\text{CCCC}}(16) + \Gamma_{\text{CCCN}}(10) + \Gamma_{\text{CCCH}}(12) + \Gamma_{\text{OCNC}}(7)$
τ_{ring}			56	0	425	$\Gamma_{\text{CCCC}}(85)$

Table 3. Mean absolute deviation, standard deviation, root mean square and correlation coefficient (r) between the calculated and observed vibrational wavenumbers of the amrinone molecule*

Parameter	IR	Raman
	DFT/wb97xd/6-311++G(d,p)	DFT/wb97xd/6-311++G(d,p)
mean absolute deviation	12.0	9.0
standard deviation	8.6	6.0
root mean square	17.2	12.0
correlation coefficient	0.9999	0.9996

*IR and Raman wavenumbers were recorded in the 4000–400 and 1700–200 cm^{-1} region, respectively.

the calculated and observed vibrational frequencies of the amrinone were given in Table 3.

2.3. Frontier molecular orbital analysis

Highest occupied molecular orbital (HOMO) and lowest unoccupied molecular orbital (LUMO) are major orbitals which are responsible for chemical reactions. The energy gap between these molecular orbitals is the measure of the kinetic stability and reactivity of the molecules and plays a major role in governing a wide range of chemical interactions. The lower the HOMO-LUMO energy gap the more reactive the molecule is [33].

The energies of the frontier molecular orbitals of amrinone were calculated by time-dependent density functional theory (TD-DFT) using wb97xd/6-311++G(d,p) basis set. The energy difference between the ground energy level and the first excited state of amrinone was found to be 4.3371 eV. The percentage of contributions of atomic orbitals in the HOMO and LUMO (frontier orbitals) was determined by applying GaussSum (Version, 3.0) software package [34]. The calculated transition energies, oscillator strengths and major contributions are given in Table S1. The 4.3371 eV energy gap between the ground electronic state and the first excited state indicates the bioactivity of the molecule. The schematic representations of the frontier HOMO and LUMO orbitals of amrinone are

shown in Fig. 3, *a*. As seen in the figure the HOMO molecular orbital is mostly localized on the 2-pyridone ring of amrinone molecule, whereas the LUMO molecular orbital is localized on the pyridine ring. In this study, the predicted frontier orbitals explain the charge transfer interaction within the molecule that influences the biological activity of the compound. In the research on milrinone the HOMO-LUMO energy gap is estimated to be 4.2142 eV by DFT/B3LYP/6-31G(d,p) calculation [7].

The density of states data (DOS) was calculated with GaussSum 3.0 software [34]. In Fig. 3, *b* the simulated density of states diagram of amrinone is shown. DOS plot is used to calculate numbers of orbitals that are available at the given energy level [35].

2.4. Molecular electrostatic potential

The molecular electrostatic potential map (MEP) shows the active sites of the molecule and is a visual interpretation of electrophilic and nucleophilic parts of the molecule. The MEP of the amrinone molecule is given in Fig. 4. In the figure the red and blue region represents the electron-rich and electron-poor regions, respectively, while the slightly electron-rich region is represented by yellow, and the slightly electron-poor region is represented by light blue.

The regions around the oxygen atom of the 2-pyridone ring and nitrogen atom of the pyridine ring were found

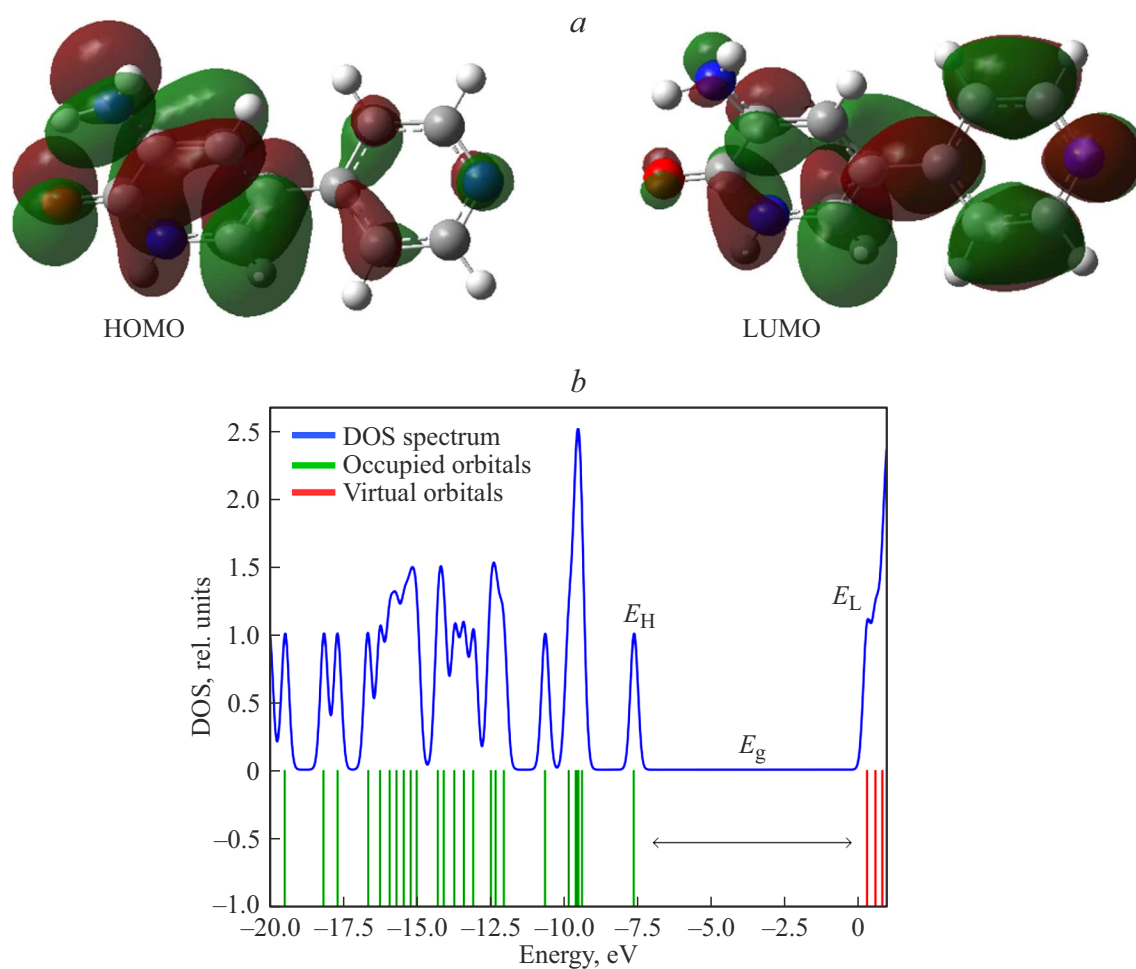


Figure 3. The pictorial representation of the HOMO and LUMO frontier molecular orbitals (a) and the density of states (DOS) diagram of amrinone (b).

$-6.268e-2$  $6.268e-2$

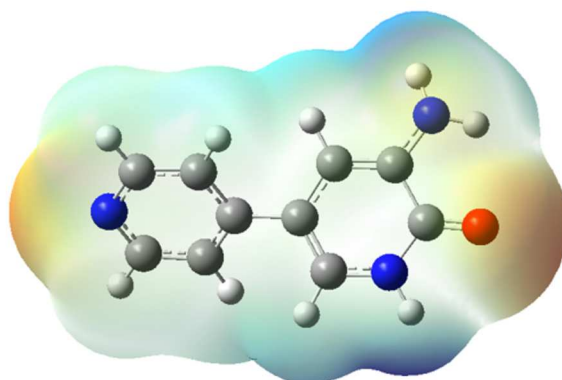


Figure 4. The molecular electrostatic potential surface (MEP) of amrinone.

to be electron-rich (red) due to the lone pairs of the oxygen and nitrogen atoms, whereas the regions around the amino nitrogen atom was found to be slightly electron-rich (yellow) because the electronegative nitrogen atom attracts

the electrons in the hydrogen atoms. Hydrogen atoms of NH and NH₂ groups, as positive potential regions, are responsible for the nucleophilic attack. On the other hand, oxygen and nitrogen atoms as negative potential regions

are responsible for the electrophilic attack. The MEP surface of amrinone changes from -0.06268 (darkest red) to 0.06268 V (deepest blue) which corresponds to an energy difference of ± 392775.58 kcal/mol.

2.5. Molecular docking analysis

2.5.1. Molecular interactions between amrinone and human phosphodiesterase 3 (PDE3B) Amrinone is a cardiotoxic agent, which increases the cyclic adenosine monophosphate level (cAMP) by inhibition human phosphodiesterase 3 (PDE3). To elucidate the behavior of amrinone as a phosphodiesterase inhibitor, the main binding interactions of amrinone with PDE3 was investigated by docking simulations. Molecular docking of amrinone is performed against the PDE3B. The human phosphodiesterase complexed with the inhibitor MERCK1 was chosen for docking studies [15] since its X-ray structure was available. The crystal structures of human phosphodiesterase PDE3B was retrieved from the Protein Data Bank (PDB). The accession code for PDE3B in complex with MERCK1 with 2.40 \AA resolution is 1SO2 [15]. The enzyme was prepared for docking by removing the existing ligand (MERCK1) and water molecules and adding polar hydrogens in it. The Kollman charges of protein were also determined. The optimized structure of amrinone was adapted for the docking. The partial charges of amrinone were calculated using the Geistenger method. The active regions of enzyme determined from previous studies were considered [36,37]. The molecular docking of the amrinone on the two active regions of PDE3B revealed 18 ligand enzyme interactions, among them the major energetically favored binding of amrinone in the active site of PDE3 was shown in Fig. 5. The interaction diagrams of amrinone PDE3 complex are also indicated in this figure. The binding affinity was found to be -7.8 kcal/mol. Amrinone presents strong binding affinity with PDE ($K_d = 1.9 \mu\text{M}$).

The details of the interaction types and distances between the amino acids of the enzyme and the amrinone molecule are given below:

2.13 \AA long hydrogen bond interaction between amino group of amrinone and TYR736,

3.71 \AA long carbon—hydrogen bond interaction between amrinone CO and GLY940,

5.31 \AA long Pi-alkyl interaction between amrinone and PRO941,

2.45 \AA long hydrogen bond interaction between amrinone CO and HIS948,

2.56 and 2.65 \AA long hydrogen bond interactions between NH and CO groups of amrinone and THR952, respectively,

4.99 \AA long and 3.82 \AA long Pi-alkyl and Pi-sigma interactions, respectively, between amrinone and ILE955,

2.36 \AA long hydrogen bond interaction between amrinone NH and GLN988,

3.83 \AA and 5.99 \AA long Pi-Pi interactions between amrinone and PHE991.

The molecular docking results indicated that amrinone interacted with PDE3 mainly by hydrogen bonding, and with small extents Pi-Pi stacking, Pi-alkyl, Pi-sigma interactions.

2.5.2. Molecular interactions between amrinone and cytochrome P450s (CYPs) Cytochrome P450 enzymes play the most important role in metabolizing pharmaceuticals. To understand the pharmacological effects of drugs *in vivo* it is important to investigate the interactions with cytochrome P450 isoforms. The activities of CYP enzymes can be modified by other compounds. As a result, using a CYP substrate in combination with a CYP inhibitor may result in decreased excretion of the CYP substrate, thus leading to adverse drug reactions or treatment failures [38–40]. As will be discussed below, the estimation of the absorption, distribution, metabolism, excretion and toxicity (ADMET) properties of amrinone predicts that amrinone is a potential inhibitor of cytochrome P450 isoforms (CYP1A2, CYP2C9 and CYP2C19). Therefore, the molecular docking studies were undergone to analyze amrinone interactions with CYP1A2, CYP2C9 and CYP2C19.

As a result of the docking simulations of amrinone with CYP1A2, CYP2C9 and CYP2C19 binding affinities are found as -8.2 , -7.0 and -6.9 kcal/mol, respectively. The 3D docked views of the most stable conformer of amrinone in CYP1A2 (A) CYP2C9 (B) and CYP2C19 (C) are given in Fig. 6. The ligand interaction diagrams of receptor-ligand complexes are also shown in the figure.

In a previous study conducted by Shao et al. (2014) the interaction of Puerarin [41], an isoflavone glycoside extracted from Pueraria plants, with CYP1A2 was investigated by docking simulations. As a result, the binding affinity was found -5.73 kcal/mol and Puerarin was found to interact Phe226, Ile314, Gly316 and Ala317 residues on α -helix as well as Phe451 and Gly459 residues on random coils. Puerarin is known to inhibit remarkably the activity of CYP1A2 [42]. In our study amrinone is found to interact with Phe 226 (Pi-Pi stacked interaction), Gly 316 (amide-Pi interaction) and Ala 317 (van der Waals interaction) residues of CYP1A2. The interaction with the same residues of the CYP1A2 indicates that amrinone entered the same active site where puerarin binds to the enzyme. Moreover, results indicated that amrinone interacted with CYP1A2 more strongly (-8.2 kcal/mol) than that of Puerarin-CYP1A2 interaction (-5.73 kcal/mol).

Amrinone has the highest tendency to bind with CYP1A2 ($\Delta G = -8.2$ kcal/mol). This is followed by the tendencies to bind with CYP2C9 ($\Delta G = -7.0$ kcal/mol) and then CYP2C19 ($\Delta G = -6.9$ kcal/mol).

2.5.3. In silico molecular docking analysis of amrinone as anticancer agent To reveal the anticancer activity of amrinone molecular docking studies were performed and interactions of amrinone with $\alpha_5\beta_1$, $\alpha_{11B}\beta_3$ integrins and DNA were evaluated. In the case of the

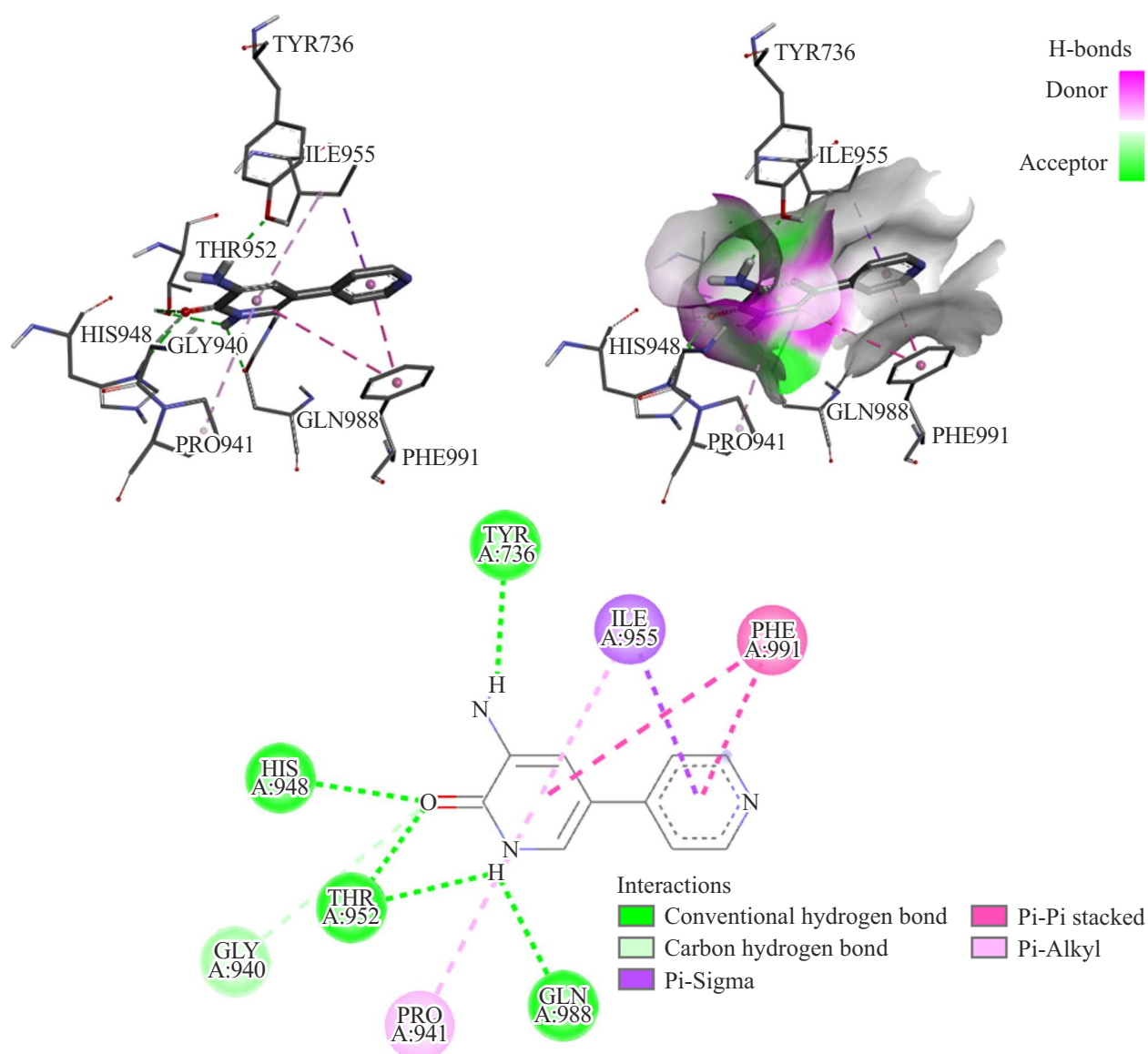


Figure 5. The 3D docked view of the most stable conformer of amrinone in human phosphodiesterase 3 (PDE3B). The ligand interaction diagrams of receptor ligand complex are shown.

investigation of the interaction of the title molecule with $\alpha_5\beta_1$ integrin (PDB ID: 4WK0), the binding probability of the ligand from two different active sites of the enzyme was examined. The molecular model of $\alpha_5\beta_1$ integrin was shown in Fig. S1, and the two active sites of $\alpha_5\beta_1$ integrin were roughly indicated by circles. The 3D docked views of the most stable conformer of amrinone in active site 1 and 2 of $\alpha_5\beta_1$ integrin are shown in Figs. 7, *a* and 7, *b*, respectively. The binding affinity of amrinone to $\alpha_5\beta_1$ integrin at active site 2 ($\Delta G = -6.6$ kcal/mol) is found to be higher than at active site 1 ($\Delta G = -6.0$ kcal/mol).

The 3D docked views of amrinone in .IIB.3 integrin (PDB ID: 3ZDX) and DNA (PDB ID: 1BNA) are given in Figs. 7, *c* and 7, *d*, respectively. The ligand interaction diagrams of receptor-ligand complexes are also shown in the figure. The molecular docking simulations of amrinone

with .IIB.3 integrin and DNA are resulted in -6.6 kcal/mol and -6.5 kcal/mol binding affinities, respectively.

The high binding affinity of the molecule to DNA and integrins suggests the use of the molecule as an anticancer agent.

2.6. Predictions of ADMET properties of amrinone

The estimated toxicity risk values and some significant physicochemical properties of amrinone were determined using OSIRIS Property Explorer (2010) [24]. The silico module admetSAR has been used to characterize the various ADMET parameters (absorption, distribution, metabolism, excretion, toxicity) for amrinone [25]. The purpose of these calculations is to show the close correspondence of the in silico predicted ADMET properties of

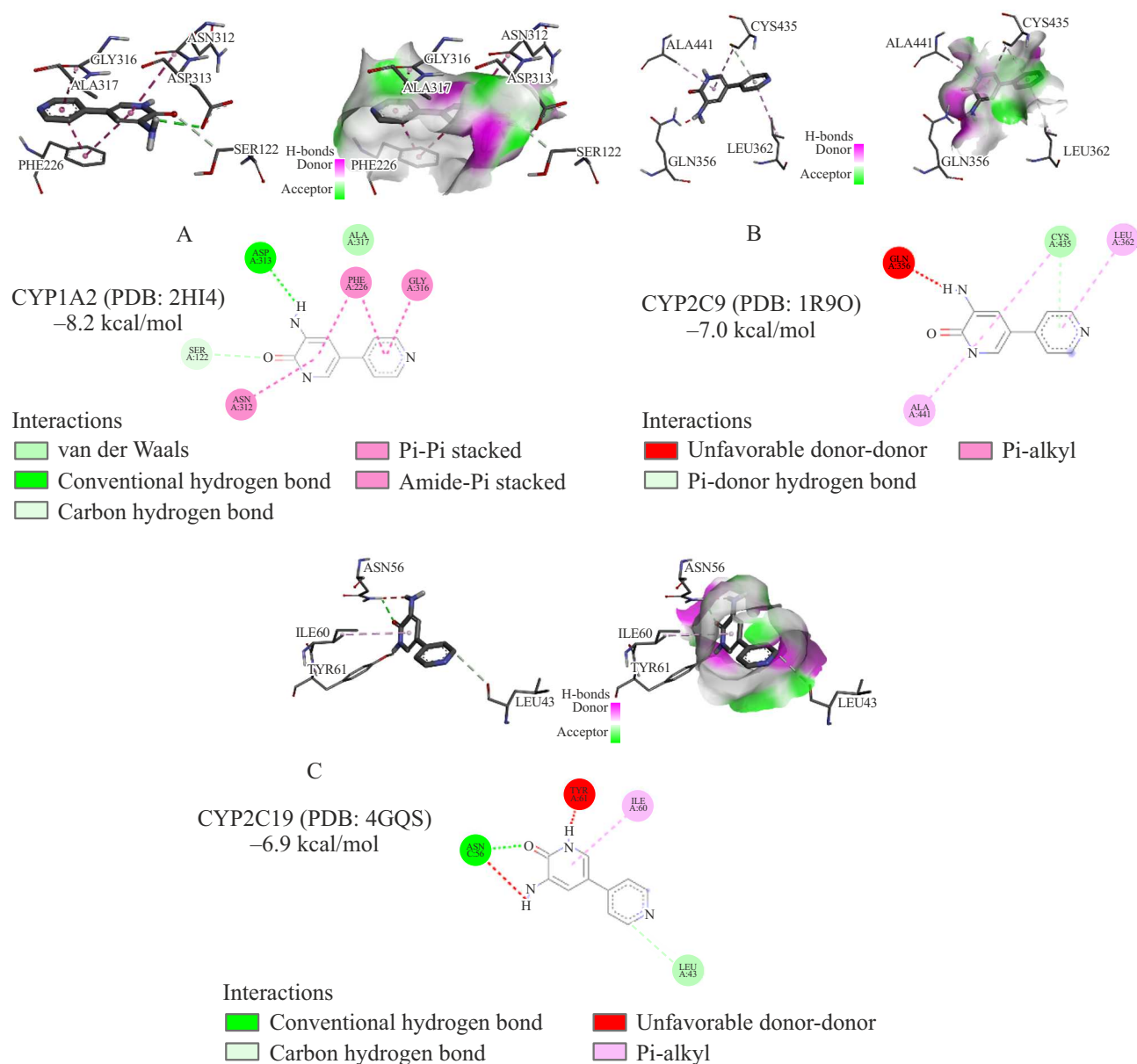


Figure 6. The 3D docked view of the most stable conformer of amrinone in human cytochrome P450 isoforms: CYP1A2 (A), CYP2C9 (B), CYP2C19 (C). The ligand interaction diagrams of receptor ligand complexes are shown.

the amrinone to its properties already known as a drug. The results are given in Tables 4 and 5. The compound was predicted to have no toxicity risk (Table 4). Bioavailability score in term of lipophilicity and aqueous solubility for a drug molecule is important. It can be seen in Table 5 that the molecular weight of the amrinone was 187 g/mol and is among the recommended values (< 500), and $clog P$ is equal to -1.01 which means that a higher affinity for the aqueous phase, so it is more hydrophilic [24]. The absorption of drugs depends on solubility and permeability [43]. Low dissolution of gastrointestinal fluids can affect the bioavailability and efficacy of the drug [43]. The solubility of a molecule is represented by $\log S$. It is an important factor, since poor solubility means poor

absorption and bioavailability. The common commercial drug's $\log S$ value is greater than -4 [24]. The $\log S$ value of amrinone is -1.27 , which means that it is soluble. The Caco-2 permeability ($\log Papp$) value of amrinone is predicted as 1.1473 cm/s. With $\log Papp > 0.9$ cm/s, so it can be predicted that the compound has a high Caco-2 permeability and is easily absorbed [44]. The AMES toxicity test can be used to assess the toxicity of the drug. The AMES test is a tool for predicting the mutagenic ability of a compound that uses bacteria [45]. The results in AMES test also suggest that amrinone may not be toxic, may be non-carcinogen and may not have biodegradation. LD stands for „lethal dose“. LD50 is the amount of a material, given all at once causes the death of 50% (one half) of a group

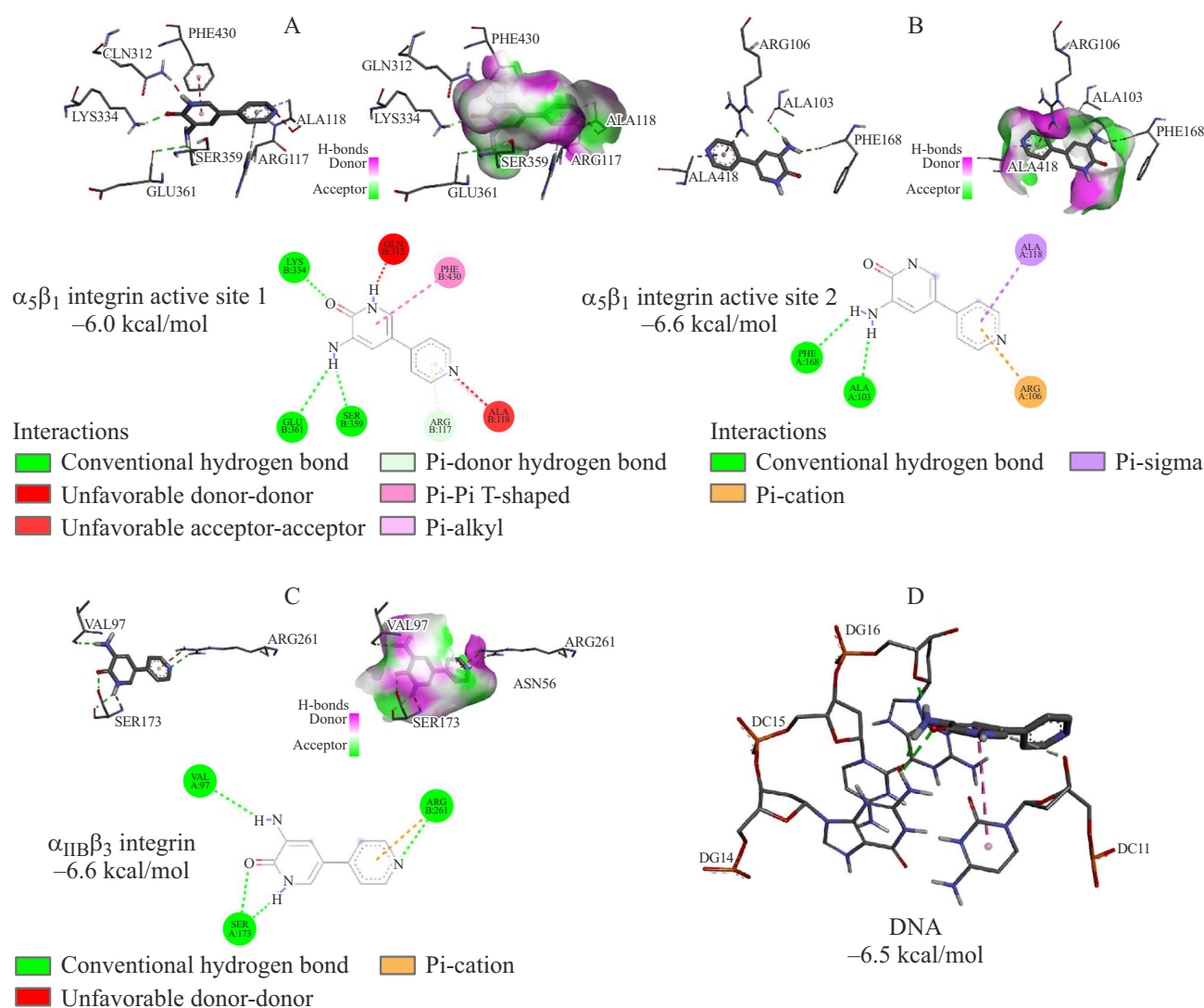


Figure 7. The 3D docked view of the most stable conformer of amrinone in active site 1 of $\alpha_5\beta_1$ integrin (A), active site 2 of $\alpha_5\beta_1$ integrin (B), $\alpha_{IIb}\beta_3$ integrin and D) DNA (C). The ligand interaction diagrams of receptor-ligand complexes and bonding affinities are shown.

Table 4. Osiris's estimation of title compounds toxicity hazards and physicochemical properties

Compound	Toxicity risks				Physicochemical properties					
	Mutagenic	Tumorigenic	Irritant	Reproductive Effect	cLog P	Solubility	MW	TPSA	Drug likeness	Drug-score
Amrinone	no	no	no	yes	-1.01	-1.27	187	68.01	0.75	0.49

of test animals [46]. The LD50 is one way to measure the short-term poisoning potential (acute toxicity) of a material.

The blood-brain barrier (BBB) is designed to shield the brain from infectious agents [47]. The BBB permeability of amrinone is found to be positive with 0.9525 probability value. The BBB+ prediction enables the bioavailability of amrinone in the brain environment, implying that amrinone may be useful for brain cancer treatment.

Cytochrome P450s (CYPs) are very important phase I metabolizing enzymes, stand out due to their effects on

drug metabolism [41]. Amrinone is predicted as inhibitor of CYP1A2, CYP2C9 and CYP2C19. Integrins play a significant role in tumor invasion and progression in glioblastomas [48].

3. Conclusion

Among the five isoenzymes of phosphodiesterase (PDE) inhibitors, amrinone is a selective PDE3 inhibitor. By inhibiting the cellular phosphodiesterase of the myocardium,

Table 5. Prediction of ADMET profiles of theamrinone

ADMET predicted profile — classification		
Model	Result	Probability
Absorption		
Blood-Brain Barrier	BBB+	0.9525
Human Intestinal Absorption	HIA+	0.9522
Caco-2 Permeability	Caco2+	0.8867
P-glycoprotein Substrate	Non-substrate	0.6469
P-glycoprotein Inhibitor	Non-inhibitor	0.9338
	Non-inhibitor	0.9946
Renal Organic Cation Transporter	Non-inhibitor	0.9258
Distribution		
Subcellular localization	Nucleus	0.6657
Metabolism		
CYP450 2C9 Substrate	Non-substrate	0.8642
CYP450 2D6 Substrate	Non-substrate	0.8389
CYP450 3A4 Substrate	Non-substrate	0.6443
CYP450 1A2 Inhibitor	Inhibitor	0.9107
CYP450 2C9 Inhibitor	Inhibitor	0.5328
CYP450 2D6 Inhibitor	Non-inhibitor	0.9651
CYP450 2C19 Inhibitor	Inhibitor	0.8994
CYP450 3A4 Inhibitor	Non-inhibitor	0.6534
CYP Inhibitory Promiscuity	High CYP Inhibitory Promiscuity	0.5933
Excretion		
Toxicity		
Human Ether-a-go-go-Related Gene Inhibition	Weak inhibitor	0.9923
	Non-inhibitor	0.7418
AMES Toxicity	Non AMES toxic	0.8492
Carcinogens	Non-carcinogens	0.9116
Fish Toxicity	High FHMT	0.6066
Tetrahymena Pyriformis Toxicity	High TPT	0.6568
Honey Bee Toxicity	Low HBT	0.8927
Biodegradation	Not ready biodegradable	1.0000
Acute Oral Toxicity	II	0.6057
Carcinogenicity (Three-class)	Non-required	0.6351
ADMET predicted profile — regression		
Model	Value	Unit
Absorption		
Aqueous solubility	-2.2573	LogS
Caco-2 Permeability	1.1473	LogPapp, cm/s
Toxicity		
Rat Acute Toxicity	2.9371	LD50, mol/kg
Fish Toxicity	2.0609	pLC50, mg/L
Tetrahymena Pyriformis Toxicity	0.2098	pIGC50, ug/L

it causes cAMP to increase at the cellular level, which facilitates the contraction of myocardial cells [1]. To elucidate the interaction mechanism of amrinone with PDE3, molecular modelling study on amrinone molecule was performed. The most stable geometry of amrinone

was predicted at DFT/wb97xd/6-311++G(d,p) level of theory. The vibrational spectra of amrinone were analyzed according to the agreement between the calculated and observed results. Molecular docking approach was applied to understand the interaction of the amrinone with the

PDE3. The binding energy of amrinone against PDE3B was found to be -7.8 kcal/mol. The result shows that amrinone presents strong binding affinity for PDE3B. Moreover the molecular docking studies revealed the strong interaction between amrinone and DNA, $\alpha_5\beta_1$ and $\alpha_{11B}\beta_3$ integrins (-6.5 , -6.6 and -6.6 kcal/mol, respectively), which allowed us to predict it as an anticancer agent. The findings shed light on the pharmacological profile of amrinone.

Funding

This study was supported by the Research funds of Istanbul University (ÖNAP-2423).

Conflict of interest

The authors declare that they have no conflict of interest.

References

- [1] R.S. Vardanyan, V.J. Hruby. *Synthesis of Essential Drugs*, Ch. 17 (Elsevier, 2006). doi.org/10.1016/B978-0-444-52166-8.X5000-6
- [2] M. Asif, North American J. Med. Sci. **4**(10),499 (2012).
- [3] G. Pastelin, R. Mendez, E. Kabela, A. Farah. Life Sci. **33** (18), 1787 (1983).
- [4] D.W. Robertson, E.E. Beedle, J.K. Swartzendruber, N.D. Jones, T.K. Elzey, R.F. Kauffman, H. Wilson, J.S. Hayes. J. Med. Chem. **29** (5), 635 (1986).
- [5] H.J. Hofmann, R. Cimiriaglia. Eur. J. Med. Chem. **22** (6), 569 (1987).
- [6] V. Cody. Acta Crystallographica C **43** (7), 1325 (1987).
- [7] A. Esme. Indian J. Pure & Appl. Phys. **55** (7), 478 (2017).
- [8] Y. Shao, L.F. Molnar, Y. Jung, J. Kussmann, C. Ochsenfeld, S.T. Brown, R.A. Di Stasio Jr. Phys. Chem. Chem. Phys. **8** (27), 3172 (2006).
- [9] M.J.E.A. Frisch, G.W. Trucks, H. Schlegel, G.E. Scuseria, M.A. Robb, J.R. Cheeseman et al. (2004). Gaussian 03, revision c. 02; Gaussian, Inc., Wallingford, CT, 4.
- [10] A.D. Becke. J. Chem. Phys. **98** (7), 5648 (1993).
- [11] P. Pulay, G. Fogarasi, G. Pongor, J.E. Boggs, A. Vargha. J. Am. Chem. Soc. **105** (24), 7037 (1983).
- [12] T. Sundius. J. Mol. Str. **218**, 321(1990).
- [13] T. Sundius. Vibr. Spectr. **29** (1), 89 (2002).
- [14] K. Istvan, (2002). SIMIRRA — program for simulation of IR and Raman spectra. Budapest: Chemical Research Center. (It was obtained from Dr. Gabor Keresztury in Chemical Research Center in Budapest).
- [15] G. Scapin, S.B. Patel, C. Chung, J.P. Varnerin, S.D. Edmondson, A. Mastracchio et al., Biochemistry **43** (20), 6091 (2004).
- [16] H.R. Drew, R.M. Wing, T. Takano, C. Broka, S. Tanaka, K. Itakura, R.E. Dickerson. Proc. National Acad. Sci. **78** (4), 2179 (1981).
- [17] W. Xia, T.A. Springer. Proc. National Acad. Sci. **111** (50), 17863 (2014).
- [18] J. Zhu, J. Zhu. J. Cell Biol. **201** (7), 1053 (2013).
- [19] S. Sansen, J.K. Yano, R.L. Reynald, G.A. Schoch, K.J. Griffin, C.D. Stout, E.F. Johnson. J. Biol. Chem. **282** (19), 14348 (2007).
- [20] M.R. Wester, J.K. Yano, G.A. Schoch, C. Yang, K.J. Griffin, C.D. Stout, E.F. Johnson. J. Biol. Chem. **279** (34), 35630 (2004).
- [21] R.L. Reynald, S. Sansen, C.D. Stout, E.F. Johnson. J. Biol. Chem. **287** (53), 44581 (2012).
- [22] O. Trott, A.J. Olson. J. Comp. Chem. **31** (2), 455 (2010).
- [23] A. Jurcik, D. Bednar, J. Byska, S.M. Marques, K. Furmanova, L. Daniel, P. Kokkonen, J. Brezovsky, O. Strnad, J. Stourac, A. Pavelka, M. Manak, J. Damborsky, B. Kozlikova. Bioinformatics, **34**, 3586 (2018).
- [24] OSIRIS. (2010). OSIRIS Property Explorer. Actelion Pharmaceuticals Ltd. <http://www.organic-chemistry.org/prog/peo/>
- [25] F. Cheng, W. Li, Y. Zhou, J. Shen, Z. Wu, G. Liu, P.W. Lee, Y. Tang, J. Chem. Inf. Model. **52** (11), 3099 (2012).
- [26] A.K. Bhattacharjee. Proc. Indian Acad. Sci. (Chem. Sci.) **102** (2), 159 (1990).
- [27] H.D. Arman, P. Poplalkhin, E.R. Tiekink. Acta Crystallographica E **65** (12), o3187 (2009).
- [28] S. Castillo, J. Favrot, T. Bouissou, J.F. Brazier, M.T. Boisdon, A. Zwick. Spectrochimica Acta A, **50** (6), 1121 (1994).
- [29] T. Nakanaga, F. Ito, J. Miyawaki, K. Sugawara, H. Takeo. Chem. phys. lett. **261** (4–5), 414(1996).
- [30] J.C. Evans. Spectrochimica Acta **16**(4), 428(1960).
- [31] Z. Niu, K.M. Dunn, J.E. Boggs. Molecular Physics **55** (2), 421 (1985).
- [32] L. Corrsin, B.J. Fax, R.C. Lord. J. Chem. Phys. **21** (7), 1170 (1953).
- [33] R.G. Pearson. Hard and soft acids and bases. V. 2 (Van Nostrand Reinhold, NY, 1973).
- [34] N.M. O'boyle, A.L. Tenderholt, K.M. Langner. J. Comp. Chem. **29** (5), 839 (2008).
- [35] A. Atilgan, S. Yurdakul, Y. Erdogdu, M.T. Gulluo.lu. J. Mol. Struct. **1161**, 55(2018).
- [36] D.R. Martins, F. Pazini, V. de Medeiros Alves, S.S. de Moura, L.M. Liao, M.T.Q. de Magalhaes et al., Chem. Pharm. Bull. **61** (5), 524(2013).
- [37] C. Kontogiorgis, O. Nicolotti, G.F. Mangiatordi, M. Tognolini, F. Karalaki, C. Giorgio et al. J. Enz. Inh. Med. Chem. **30** (6), 925(2015).
- [38] U.M. Zanger, M. Schwab. Pharmacol. Therapeut. **138** (1), 103 (2013).
- [39] Z. Bibi. Nutr. Metabol. **5**, 27 (2008).
- [40] A.M. McDonnell, C.H. Dang. J. Adv. Pract. Oncol. **4** (4), 263 (2013).
- [41] J. Shao, J. Chen, T. Li, X. Zhao. Molecules **19**, 4760 (2014).
- [42] Q.B. Wang, W. Di, X.L. Cheng, P.H. Zhang, Z.L. Tu. Herald Med. **5**, 500 (2008).
- [43] K.T. Savjani, A.K. Gajjar, J.K. Savjani, Int. Schol. Res. Not. **2012** (2012). DOI: 10.5402/2012/195727
- [44] S. Hardjono, S. Siswandonno, R. Andayani, Indones. J. Biotechnol. **22** (2), 76 (2017).
- [45] S. Maloy, K. Hughes, (Eds.) Brenner's encyclopedia of genetics (Academic Press, 2013).
- [46] P. Wexler. Encyclopedia of Toxicology (Academic Press, 2014).
- [47] S. Brem, K.G. Abdullah. Glioblastoma (Elsevier, 2017).
- [48] L. Malric, S. Monferran, J. Gilhodes, S. Boyrie, P. Dahan, N. Skuli, J. Sesen, T. Filleron, A. Kowalski-Chauvel, E.C.J. Moyal, C. Toulas, A. Lemarie, Oncotarget **8**, 86947 (2017).